A hybrid energy storage solution based on supercapacitors and batteries for the grid integration of utility scale photovoltaic plants

Francisco Díaz-González, Cristian Chillón-Antón, Marc Llonch-Masachs, Samuel Galceran-Arellano, Joan Rull-Duran, Joan Bergas-Jane, Eduard Bullich-Massagué

Centre d'Innovació Tecnològica en Convertidors Estàtics i Accionaments (CITCEA-UPC), Department of Electrical Engineering, Universitat Politècnica de Catalunya ETS d'Enginyeria Industrial de Barcelona, C. Avinguda Diagonal, 647, Pl. 2, 08028 Barcelona, Spain

Abstract

This paper presents a 2-level controller managing a hybrid energy storage solution (HESS) for the grid integration of photovoltaic (PV) plants in distribution grids. The HESS is based on the interconnection of a lead-acid battery pack and a supercapacitor pack through a modular power electronics cabinet. The inclusion of the HESS into the PV plant –and not an state-of-the-art energy storage system based on a single technology–, is motivated by the diversity of technical requirements for the provision of the services of grid peak power shaving and PV output power ramp limitation. The 2-level controller ensures a synergistic exploitation of the two storage technologies aiming for an optimal service level of the HESS and minimum battery degradation. The higher level of the controller is based on a mathematical optimization problem that solves with the optimal schedule of the storage technologies for peak power shaving purposes. The power setpoints of this optimization are then complemented by a real time controller managing PV plant output ramp limitation. The HESS performance and associated controller has been proved effective through two case studies. The first one adopts a 6.6 MW PV plant including a HESS solution combining a 5.5 MWh and 2.64 MW lead-acid battery pack with a 0.25 MWh and 1.32 MW supercapacitor pack. The second one reports experimental data from an analogous scenario scaled down to kW level and using a laboratory scale prototype for the HESS. All in all, the hardware and software solutions proposed in this paper contribute to a feasible exploitation of multi-purpose energy storages targeting the needs of renewables' and distribution system operators.

Keywords: Hybrid Energy Storage Solution, Battery, Supercapacitor, PV plant, Power electronics

1. Introduction

The installation of renewable generation presents a growing tendency worldwide over the last decades, being mainly motivated by the need for reducing the dependency from fossil fuels and coal, as well as the required decrease of pollutant emissions. According to IRENA (International Renewable Energy Agency) [1], at the end of 2019, global renewable generation capacity was 2351 GW, dominated by hydro (1172 GW), wind (564 GW) and solar (486 GW). More than 80 % of the new capacity that was built in 2018 came from solar and wind installations. Therefore, it is clear wind and PV power plants play a key role for contributing to the power system decarbonisation. However, their power output is variable and unpredictable to some extent, and this is a barrier for their grid integration that motivates the association of Energy Storage Solutions (ESSs).

The focus of this paper is on mid-scale ESS and, in particular, on hybrid ESS (HESS). A HESS combines different energy storage technologies in a single device so as to benefit from the technical and economic

Email address: francisco.diaz-gonzalez@upc.edu (Francisco Díaz-González)

advantages each one can offer depending on the performance required in different operational situations. Depending on the type of storage technology activated, a HESS could optimally exchange large amount of energy but at reduced power, exploiting for instance a low cost secondary battery; and trigger a complementary storage technology like a supercapacitor pack for providing high power for a very short time, thus diminishing battery degradation and improving overall dynamic performance. All in all, the concept of hybridization is seen as a solution to overcome one of the main barriers of conventional ESSs: there is no a single technology (e.g. a battery, a supercapacitor, a flywheel) offering optimal performance for everything.

Literature on the services ESSs can provide in electrical grids is extensive [2]. While small-scale ESSs are associated to the end user domain, offering services for individual or community self-consumption, mid and large-scale ESS are focused to the operation of transmission and distribution networks, utility scale renewables as well. Distributor System Operators (DSOs) are in charge of ensuring a reliable supply to the connected customers and with a proper level of power quality. The services offered by a DSO are not market-based but determined, bounded and remunerated following the rules and definition of competences in the electrical sector. In Europe, for instance, these are stated in the Directive 2019/944.

This has a relevant impact when it comes to a DSO to operate an energy storage system: the energy exchanged by a battery under a DSO command cannot be exploited in electrical markets. As a result, applications of energy storages under this category and concerning DSOs refer to the technical optimization of DSO services to end users. For instance: over and under voltage control, load unbalance compensation among the three-phase systems of grids, correction of flicker and current harmonics, load congestion alleviation in electrical infrastructure and security of supply for customers at district or neighbourhood level.

In regard of utility scale renewables, the aim of an ESS here, is to make the output of wind and PV plants more and more controllable and predictable. Mimicking the behaviour of large synchronous generators means, in practice, to make renewables to participate in system ancillary services. Conventionally, some of these services, such as the provision of frequency containment reserves (formerly known as primary reserves) for grid frequency control are market-based. Others, on the contrary, are just mandatory and considered as a prerequisite for a power plant to be connected to the grid, such as voltage control through reactive power compensation and power ramp limitation. The contribution of energy storage in renewable-based systems draws clear business cases to explore.

1.1. Motivation of the work

The challenge of simultaneously provide services to various agents.- For an energy storage operator, it is hard to ensure the economic feasibility of a business pivoting on the provision of just one service to a particular stakeholder. Therefore, the stacking of services is principal but this poses various challenges to face as: i) various stakeholders may be involved and these may be non market-based, e.g. a DSO, or market-based as those in the field of generation and commercialization of electricity - regulatory boundaries; ii) the services provided may be contradictory and consider different time scales; iii) the identification and valorization of the energy associated to each service.

Work in [9, 3, 4] discuss on the aspects above. Remarkable work is reported in [4], as proposing a new business model for the operation of a centralized storage unit and shared among TSO, renewable generators and consumers. The allocation of the power and energy needs from the battery is based on explicit auctioning. The optimization objective of each of the players is obviously different: consumers try to capture differences in electricity price; renewables try to maximize the market value of its generation; and the TSO aims to minimize power imbalances through power reserve allocation. The combination of storage resource rights for each player is orchestrated and solved as the generalized Nash equilibrium problem. The mechanism allocates the limited storage resources to the most valuable application for each market-clearing price, based on the competing players' willingness-to-pay.

The above mentioned work assumes that thanks to the auction, each player or stakeholder can identify part of the power exchanged by the battery, thus pay for this accordingly. The power of the battery is somehow packetized. This packetization is also proposed in [5], now through blockchain technology. The authors argue that blockchain acts as an automated aggregator, thus reducing the associated cost of an aggregator managing the auctions in [4].

An alternative to previous approaches is the adoption of a multi-objective optimization function. This can consider individual optimization function as equal in importance, as in [6], which addresses a power loss minimization in grids or a minimum transformer loading with also minimum battery size and degradation; or as weighted addressing specific goals as in [7]. In this paper, a management algorithm for a building with battery storage, PV generation and controllable loads is evaluated. The individual optimization criteria are diverse (8 functions) covering technical, economic and environmental aspects. Pareto representation technique is utilised for assessing the performance of the optimization and find optimal trade-off compromises among optimization variables. In line with the previous work, [8] proposes a multi-objective optimization also in a grid connected building equipped photovoltaics and battery storage. One of the drawbacks of multi-objective optimization with weighted individual functions is that it may result into procedures with relevant cost in terms of computational process. However, it eases the association of a cost to the degradation of the battery in comparison to strategies based on orchestrated auctions as previously discussed, and this is an added value for the energy storage owner.

The adoption of any of the techniques above for the optimization of the operation of ESS is hindered by aspects such as the stochastic nature of data associated to consumption and generation time profiles, the uncertainty in model parameters for the technologies involved in the systems to optimize as well. To cope with these matters, diverse techniques are proposed in literature as rolling horizon optimization [10], Markov-based decision process [11], particle swarm optimization [12] and Monte Carlo simulations [13], among many others. Even further, the complexity of optimizing the operation of storages increases while considering active and reactive power flows. This implies a more detailed model of the battery and the electrical system it is connected to, as discussed in [15, 14].

The challenge of simultaneously exploit various storage devices embedded into a hybrid solution.- The applications previously described request energy storages to either react almost instantaneously to exchange a relevant power during a short time (e.g. the case of the provision of frequency containment reserves for system frequency control) and to absorb or inject a sustained amount of power for a prolonged period of time (e.g. the case of domestic or community self-consumption). The most suitable storage technologies for power services could be, for instance, flywheels, supercapacitors or batteries with limited degradation under conditions of high stress with respect of the current exchanged, as the case of lithium-ion ones. Complementary, the most suitable technologies for energy services could be, for instance, low cost batteries with respect to energy storage capacity such as lead-acid ones, more and more lithium-ion and even flow batteries. There is no an energy storage system based on a single technology, that results optimal in terms of economics and technical performance while providing both energy and power services. The concept of hybridization of energy storages –addressed here as the twinning of various storage technologies– arises as a strategy to develop sustainable, high performance and cost competitive ESSs, with the potential of definitely decarbonizing stationary ends. However, to exploit and obtain the best of each of the storage technologies composing the hybrid solution, advanced power sharing algorithms should be embedded in.

The power sharing capability depends on factors related to how various storage devices are interconnected in the hybrid solution and the algorithms managing power in and out. About the latter, there can be found hybrid storage solutions opting for active and passive parallelization [16, 17]. Passive means that, for instance, a supercapacitor and a battery are directly interconnected, so no power converters are interfaced in between. At the circumstance of receiving a power demand, part of the total current drawn by the assembly would be provided by each storage device, and this would depend on the intrinsic parameters of each one. There is no specific control on the transient response of each storage device, neither on the amount of power provided by each one. This way, the operational flexibility is not maximized. Conversely, an active interconnection of storage devices, e.g. the parallelization of a battery and a supercapacitor through dedicated dc-dc converters sharing a common dc-link, eases the independent operation of each storage device, thus exploiting the main performances of each one. This is a more complex and costly strategy, though.

Concentrating now on options relying on active hybridization and addressing algorithms, the main question is to decide on how to distribute power demand among the different storages embedded in. To do so, some works opt for filtering out the net power demand profile to identify, for instance, the high frequency components to associate to a supercapacitor, thus exploiting the high ramp power rates and cyclability of this technology; and the low frequency components that could be requested from a battery, thus reducing

cycling stress and extending lifespan. An example of this strategy is the research in [18], where the power demand corresponds to the needs of the inverter driving the motor of an electrical vehicle. An interesting –and associated question– to the filtering of power demand in this paper is the manner of determining this power demand, since based on the application of a robust H∞ controller on the voltage of the common dc link interconnecting the dc-dc converters of the storages and the main inverter. Another example on the strategy of filtering out the net power demand for a hybrid storage solution is found in [19], now addressing a stand-alone PV-based micro-grid. The net power demand profile is stratified into three components in this paper: high, medium and low frequency power fluctuations. Components are associated to a supercapacitor, lithium-ion and lead-acid battery, respectively, addressing their dynamic performance.

An alternative to the application of traditional low-pass and high-pass filters to identify what part of the net power demand should be associated to each storage device embedded into the hybrid solution is the application of the wavelet transformation, as in [20]. This paper, again addressing the application of a supercapacitor-battery hybrid solution in electrical vehicles, adds a second decision level after the filtering of power demand. This is a neural network supervising driving patterns to obtain slow variations for battery power demand correction to extend lifetime, and finally a fuzzy logic block to ensure that the supercapacitor voltage is maintained within admissible limits. The inputs of the fuzzy logic are the power demand to the battery and the voltage of the supercapacitor, and the output is the excessive power added to the supercapacitor for power correction.

The idea of using a fuzzy logic as a decision algorithm is also applied in [21, 22]. Work in [22], researches on the problem of sharing the power demand of a micro-grid among a hybrid storage system composed by various batteries and supercapacitors connected in parallel to a common dc link. Addressing the SOC of each battery and the total current demand of the micro-grid, a fuzzy logic algorithm distributes it among the storages. As in [20], this is a two level management strategy, since the output of the power sharing algorithm (i.e. the fuzzy logic scheme) is the input for a low level management layer that actually redistributes the demand among the batteries and supercapacitors based on their instantaneous SOC to avoid over-charge and over-discharge.

The advantage of using fuzzy logic over other conventional control approaches is that there is no need to accurately model the plant or system to control, e.g. no need to know the internal resistance of a battery to tune the current controller of a dc-dc converter connected to it. One drawback though, is the involved computational cost, and this is specifically addressed in [23]. In particular, this paper deals with the problem of ensuring electrical stability of a micro-grid smoothing out power fluctuations of a wind-diesel system. At the highest decision level for a hybrid storage solution including supercapacitors and batteries, there is a proportional-derivative (PD) controller that determines the power to be exchanged by the hybrid solution as a whole to compensate frequency deviations. The parameters of this PD controller are dynamically tuned by a fuzzy logic and in combination with a PSO algorithm to reduce fuzzy system effort and computational cost. Once the power demand is determined, a low level control algorithm is proposed to distribute total effort among the supercapacitor and the battery. This algorithm also aims to avoid deep discharge and over charge for the battery and power stress. To do so, the algorithm is based on cascaded PI controllers aiming to maintain constant the common dc-link interfacing the dc-dc converters of the supercapacitor and the battery with the micro-grid.

Finally, completing this short review on power sharing strategies, works in [24, 25, 26, 27] propose relatively –but effective– heuristics that, primarily based on the SOC and the required time response, split the net power demand among the different storages embedded into the hybrid solution. For instance, [24] splits power demand based on the SOC of a battery and a supercapacitor. Both storages are connected to a common dc-link, in which a PV system and the loads of a microgrid are also attached. The need of charging and discharging the storages is from the evaluation of such dc-link voltage variations. Once distributed, the current controllers of both the battery and supercapacitor dc-dc converters ensure charge and discharge needs. The current controller of the dc-dc converter of the supercapacitor ensure faster response than that of the battery because of the fine tunning of its parameters. Similarly, in [25], an heuristic decision algorithm decides on distribute proportionally the total demand among a supercapacitor and a battery for grid frequency control purposes, based on their particular SOC and SOH impact. An additional control loop is added to slowly correct the average SOC of the battery to maintain the required power reserve in case of

a severe frequency disturbance in the grid. And finally, in [26] the power sharing among a supercapacitor and a battery for ramp rate control in a PV plant is solved by directly allocating all power demand to the supercapacitor till its SOC exceeds an advisable operation band; then its turn for the battery to react. Since the above mentioned works are based on SOC and SOH metrics, precise estimators should be added for proper performance, being this a particularly challenging task for batteries, as noted in [28] and [29].

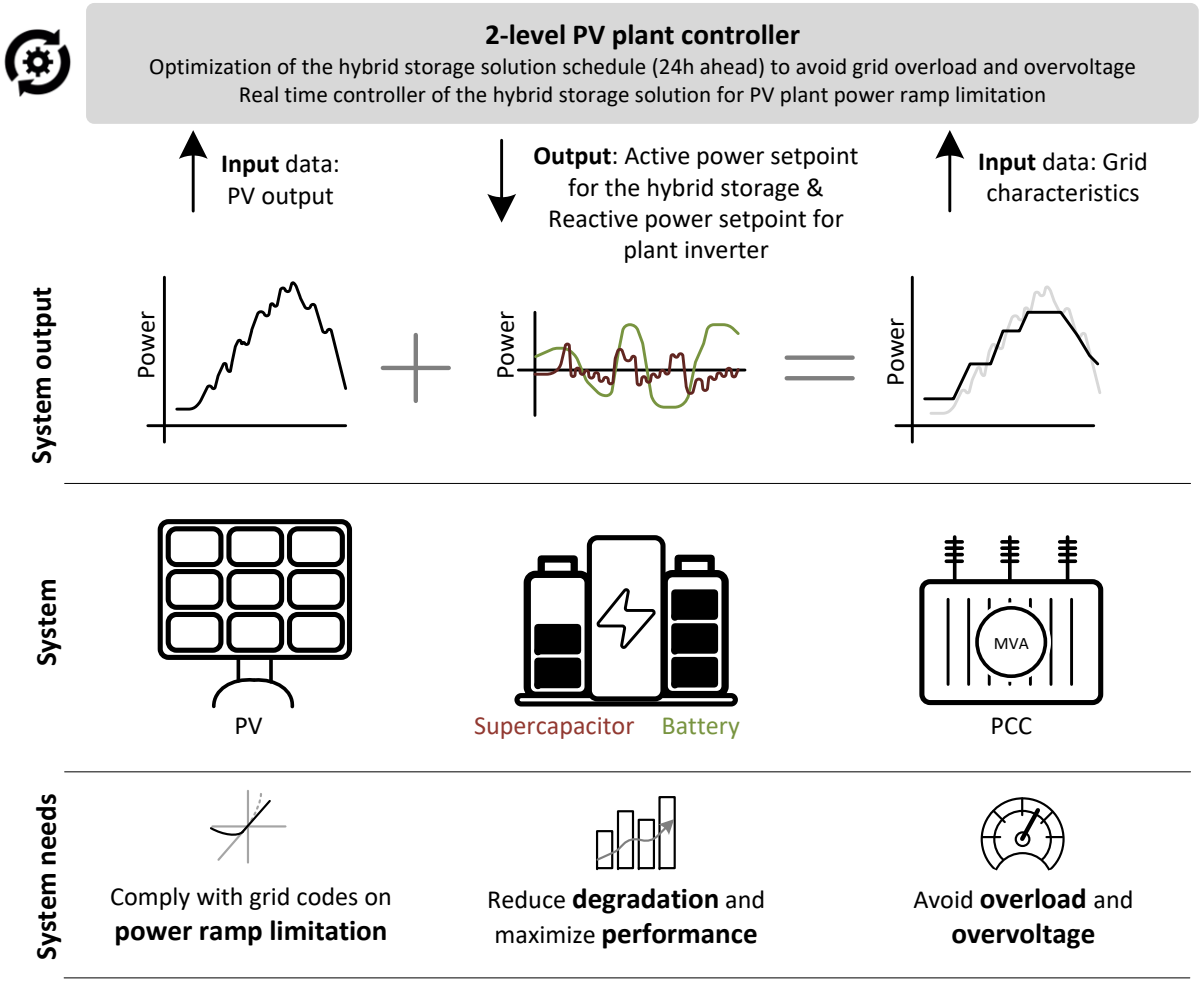

Figure 1: Scope of the work.

1.2. Contribution of the work

As identified above, the feasibility of including an ESS in an electrical network is bounded by the difficulty of providing various services at the same time and for different agents. These services, in turn, impose various performance in terms of energy storage capacity, time response and cyclability, among others. Such variety of technical requirements suggest the adoption of HESSs but, the synergistic exploitation of each storage technology configuring the hybrid solution requires advanced management strategies. The state-of-the-art review suggested techniques like blockchain, auction-based distribution of storage rights and multi-objective optimization problems to solve the simultaneous provision of services by an ESS. In turn, the state-of-the-art review on the exploitation of HESSs turned out a variety of power sharing techniques such as those based

on the filtering –the stratification– of the total power demand, robust H∞ controllers, fuzzy logic and other control schemes based on ad-hoc heuristics.

The main contribution of the paper is the formulation and validation of a novel control method for exploiting a HESS for the simulatenous provision of two services to a PV plant while also minimizing the degradation of the storage devices embedded in. The challenge of providing various services at the same time are solved by a 2-level PV plant controller. The higher level is constituted by a multi-objective optimization problem. The aim of this optimization is to solve with the optimal schedule for the storage technologies embedded into the HESS to limit peak power exchanged at the grid point of common coupling (PCC). This is to limit overvoltage in case PV generation exceeds the ratings of the grid. Thus, this service eases the grid integration of the PV plant deferring new investments for grid reinforcement. This way, the proposed method permits to tackle the optimal operation of a HESS included in a PV plant, addressing the needs of other agent apart from the PV operator, which is the network operator. In this paper, the HESS integrates a cheap lead-acid battery pack and a supercapacitor pack. For the provision of the service of peak power shaving, the HESS would exchange power during some hours continuously, so it will be the lead-acid pack the main storage technology exploited, with just some contribution from the supercapacitor to reduce battery stress.

The lower level of the PV plant controller is a real time controller limiting power ramp of the PV plant. This is one of the requirements that renewables should fulfil for grid integration according to grid codes (e.g. the EU Commission Regulation 2016/31 [30]). The provision of this service require a fast response from the HESS, derived from the stochastic and continuously varying profile of PV generation. Thus, the approach cannot be based on scheduling power setpoints based on PV generation forecasts, as in the optimization problem stated above, but a real time, reactive controller should be adopted. As a difference with other approaches in literature, nor fuzzy logic, neither power demand filtering techniques are adopted, but an ad-hoc heuristic is proposed instead. The continuous cycling and fast reaction required for power ramp limitation suggests to prioritize the exploitation of the supercapacitor. The lead-acid battery would contribute in case of reaching supercapacitor limits. Figure 1 graphically depicts the scope of the 2-level PV plant controller.

The proposed 2-level PV plant controller is superior over related literature by the fact that the constraints of the mathematical formulation founding the optimization problem not only address energy and power balances, as usually tackled at the time of scheduling the output of manageable generation or consumption assets in grids, but explicitly evaluate grid voltage and current stress. This permits to precisely solve with the best schedule in terms of both active and reactive power for HESS active power exchange and PV plant inverters. The second aspect supporting the wellness of the proposed controller is the fact that control duties are distributed over the two levels of its architecture and in accordance to the required computational effort. This way, the service of grid power peak shaving –associated to a potential daily grid overload, phenomena that, in turn, occurs for some hours and does not require a reactive, instantaneous response, but a sustained power provision from the HESS– is solved through an optimization algorithm (higher level of the controller) that has enough time to deal with the relatively large amount of data to process on grid characteristics, PV output and HESS state. On the other hand, the service of power ramp rate limitation –associated to the stochastic fast fluctuations of the PV output profile– is solved through a real time algorithm (lower level of the controller) accounting on minimum computational burden. Finally, one drawback of the proposed 2-level PV plant controller is about the tuning of the parameters based on the actual characteristics of the HESS (e.g. energy storage capacity, power limitations, voltage measurements as well). So to some extent, it is needed to properly characterize the system to control, which is no fundamental adopting other approaches in literature as, for instance, those based on fuzzy logic.

2. Methodology: A PV plant controller for a HESS providing peak power shaving and power ramp limitation

The higher level of the PV plant controller, i.e. the optimization algorithm for peak power shaving purposes, is introduced in Section 2.1. In turn, the lower level, i.e. the real time controller for power ramp limitation, is introduced in Section 2.2.

2.1. Optimization algorithm: grid peak power shaving

The higher decision level of the PV plant controller is for splitting power demand among the battery and the supercapacitor for grid peak power shaving purposes. This constitutes an optimization algorithm (in fact, a Non-Linear-Problem, NLP) that, based on the forecasts on PV generation for a predefined period of time, e.g. the next 24 hours; grid limitations and the state of charge and technical performance of the HESS, schedules the power setpoints for the supercapacitor and the battery packs. As previously explained in Section 1.2, the main storage device operated here is the battery pack, since hosting most of the energy storage capacity of the HESS. This is a result derived from the basis of the NLP presented in the following contents.

2.1.1. Input data

The input data for the optimization problem is divided into sets and parameters, see Table 1.

Table 1: Input data

Item	**Description**
T	Set for time period $T = 1, .., t_f$.
I	Set for storage units $I = 1, .., i_f$.
T_s	Time step for optimization, in h.
P_{r_i}	Rated power for storage i, in MW.
E_{r_i}	Rated energy for storage i, in MWh.
$P_{pv,t}$	PV power at time t, in MW.
ε	Maximum discrepancy between initial and final state of charge for storage technologies, in p.u.
SOC_{max_i}	Maximum admissible state of charge for the storage technology i, in p.u.
SOC_{min_i}	Minimum admissible state of charge for the storage technology i, in p.u.
η_{in_i}	Charge efficiency for the storage technology i, in p.u.
η_{out_i}	Discharge efficiency for the storage technology i, in p.u.
C_{d_i}	Degradation cost in terms of the power magnitude exchanged by the storage technology i, in p.u.
E	Nominal phase-to-phase RMS grid voltage, in kV.
R	Grid Thevenin resistance, in Ohm.
X	Grid Thevenin reactance, in Ohm.
$I_{g_{max}}$	Rated RMS grid current, in kA.
$I_{pv_{max}}$	Rated RMS current at grid point of connection due to PV installed power, in kA.
ε_v	Maximum discrepancy between the nominal and actual line voltage, in p.u.
k_g	Factor limiting the maximum power exchanged with the grid by the PV plant, in p.u.
k_{p_i}	Factor limiting the power that the storage i can develop, in p.u.
α	Weight for optimization objective of minimizing the peak power exchanged with the grid, in p.u.
β	Weight for optimization objective of minimizing storages' degradation because of power stress, in p.u.

2.1.2. Decision variables

The NLP solves with the optimal power schedule for the battery and the supercapacitor packs for grid peak power shaving. Such goal is translated into the decision variables in Table 2.

Table 2: Decision variables

Item	Description
u_t	Voltage at the point of connection of the PV plant, in kV.
$p_{i,t}$	Power exchanged by the storage technology i at time t, in MW.
q_{pv_t}	Reactive power exchanged by the PV inverters at time t, in MVA.
$e_{in_{i,t}}$	Energy consumed by the storage technology i at time t, in MWh.
$e_{out_{i,t}}$	Energy discharged by the storage technology i at time t, in MWh.
$soc_{i,t}$	State of charge of storage technology i at time t, in MWh.
s_{max}	Maximum apparent power exchanged with the grid, in MVA.

2.1.3. Objective function and problem constraints

The objective of the optimization problem is to solve with the active power to be exchanged by the HESS and the reactive power regulated at the PCC of the PV plant for each time step within the considered time horizon, so as to ensure that the grid voltage and the maximum apparent power remain within admissible levels and all accounting on minimum storages' degradation. This is to minimize the value for the optimization function z,

$$\min_{(u_t, p_{i,t}, q_{pv_t}, e_{in_{i,t}}, e_{out_{i,t}}, soc_{i,t}, s_{max})} z. \tag{1}$$

The total apparent power is limited by the ratings of the central inverter of the PV plant interfacing with the grid, and the grid capacity as well. The maximum power for the battery and the supercapacitor packs are limited by the ratings of their respective dc-dc converters. The energy exchanged by these storage devices are also limited by their maximum and minimum predefined state of charge. This general picture can be graphically observed in Figure 2.

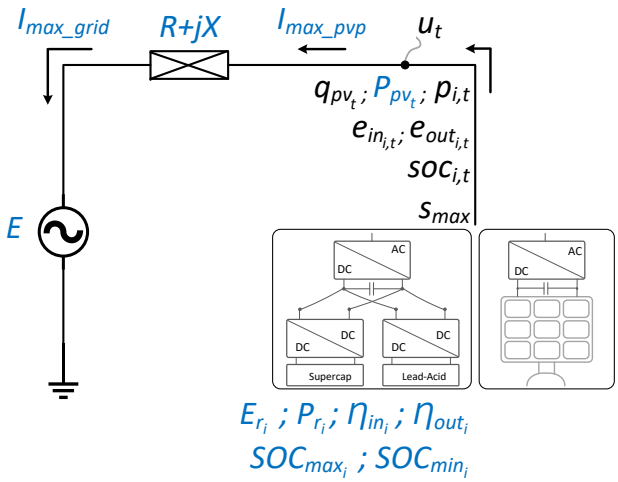

Figure 2: Graphical description of the system modelled for optimization purposes. Decision variables are noted in black, and main parameters are highlighted in blue.

As previously introduced, the optimization criteria are two-fold. Firstly, the aim is to minimize the maximum apparent power exchanged with the grid,

$$z_s = s_{max}. \tag{2}$$

Secondly, the aim is to minimize the magnitude of the peak power exchanged by the supercapacitor and the battery pack to reduce storages' degradation. To effectively capture power peaks and coherently penalise them in the optimization problem, the power profile developed by the storages is accounted as squared and

multiplied by the parameter C_{d_i}. This yields the second term of the multi-objective optimization function, z_d, as

$$z_d = \sum_{i,t} p_{i,t}^2 \cdot C_{d_i} \qquad \forall i \in I, \forall t \in T. \tag{3}$$

At the end, the optimization problem turns into a multi-objective criteria which objective function is defined as

$$z = \alpha \cdot \frac{z_s}{Z_s^*} + \beta \cdot \frac{z_d}{Z_d^*}, \tag{4}$$

where α and β are weighting factors for each of the optimization criterion, and the sum of the two factors is one. In addition, each of the optimization criterion z_s and z_d are divided by the value it takes z when considering each one as the only criterion for optimization (Z_s^* and Z_d^*, respectively). Thus, each of the optimization criterion can be fairly summed and compared between them, since levelized. This means that, the optimization should be executed three times. The first time, parameter $\alpha = 1$ and $\beta = 0$, so it is just taking into account the optimization criterion of minimizing the maximum apparent power exchanged with the grid. The obtained value for z in this first optimization is saved as Z_s^*. Then, the second execution of the optimization problem considers $\alpha = 0$ and $\beta = 1$, so just the optimization criterion of minimizing the degradation of the battery and the supercapacitor packs. The obtained value for z in this second optimization is saved as Z_d^*. Finally, once parameters Z_s^* and Z_d^* are found, the objective function z can consider simultaneously both optimization criteria, since levelized by above mentioned parameters. This, in practice, means that in this third –and last– optimization, both α and β are different from zero, each weighting the importance of minimizing the peak apparent power and the storages' degradation in the multi-objective optimization function.

The optimization function above is subjected to the following constraints. Firstly, the maximum apparent power exchanged with the grid s_{max} is calculated by

$$\sqrt{\left(P_{pv_t} + \sum_i p_{i,t}\right)^2 + q_t^2} \leq s_{max} \qquad \forall i \in I, \forall t \in T. \tag{5}$$

The apparent power is limited by the grid and ratings in the following two constraints (6) and (7), applying a security factor k_g,

$$\sqrt{\left(P_{pv_t} + \sum_i p_{i,t}\right)^2 + q_t^2} \leq \sqrt{3} \cdot u_t \cdot I_{g_{max}} \cdot k_g \qquad \forall i \in I, \forall t \in T, \tag{6}$$

$$\sqrt{\left(P_{pv_t} + \sum_i p_{i,t}\right)^2 + q_t^2} \leq \sqrt{3} \cdot u_t \cdot I_{pv_{max}} \cdot k_g \qquad \forall i \in I, \forall t \in T. \tag{7}$$

The voltage at the PCC should remain within admissible limits, thus satisfying constraint (8),

$$E \cdot (1 - \varepsilon_v) \leq u_t \leq E \cdot (1 + \varepsilon_v) \qquad \forall t \in T. \tag{8}$$

Considering above limitations, the voltage at the PCC can be solved by considering the power system in Figure 2 as a typical Thévenin circuit. Thus,

$$\left(\frac{u_t}{\sqrt{3}}\right)^4 + \left(\frac{u_t}{\sqrt{3}}\right)^2 \cdot \left[2 \cdot R \left(\frac{P_{pv,t} + \sum_i p_{i,t}}{3}\right) + 2 \cdot X \cdot \frac{q_t}{3} - \left(\frac{E}{\sqrt{3}}\right)^2\right] + \\ + (R^2 + X^2) \cdot \left[\left(\frac{P_{pv,t} + \sum_i p_{i,t}}{3}\right)^2 \left(\frac{q_t}{3}\right)^2\right] = 0 \qquad \forall i \in I, \forall t \in T, \tag{9}$$

Addressing now storages' behaviour in the following constraint, the state of charge for the storage device i at time t is expressed in terms of the energy absorbed and injected –$e_{in_{i,t}}$ and $e_{out_{i,t}}$ respectively–, and the corresponding charge and discharge efficiencies, η_{in_i} and η_{out_i}. Thus,

$$soc_{i,t} - soc_{i,t-1} = e_{in_{i,t}} \cdot \eta_{in_i} - e_{out_{i,t}}/\eta_{out_i} \qquad \forall i \in I, t \in T, \tag{10}$$

and $soc_{i,t}$ should be maintained within predetermined limits, so

$$soc_{i,t} \leq SOC_{max_i} \cdot E_{r_i} \qquad \forall i \in I, t \in T, \tag{11}$$

$$soc_{i,t} \geq SOC_{min_i} \cdot E_{r_i} \qquad \forall i \in I, t \in T. \tag{12}$$

From the energy charged and discharged by the storage device i at time t, the associated average power $p_{i,t}$ developed in this time step can be derived as

$$p_{i,t} \cdot T_s = e_{in_{i,t}} - e_{out_{i,t}} \qquad \forall i \in I, t \in T. \tag{13}$$

Power $p_{i,t}$ should not exceed the ratings for each storage device i. This is represented as

$$p_{i,t} \leq P_{r_i} \cdot k_{p_i} \qquad \forall i \in I, t \in T. \tag{14}$$

$$p_{i,t} \geq -P_{r_i} \cdot k_{p_i} \qquad \forall i \in I, t \in T. \tag{15}$$

Then, constraint (16) ensures that the storage device i is not charged and discharged simultaneously,

$$e_{in_{i,t}} \cdot e_{out_{i,t}} = 0 \qquad \forall t \in T. \tag{16}$$

Constraint (17) ensures that the difference between the initial and final state of charge for each storage device is almost equal –assuming a small discrepancy represented by parameter ε–,

$$(1-\varepsilon) \cdot soc_{i,1} \cdot E_{r,i} \leq soc_{i,T}(1+\varepsilon) \cdot soc_{i,1} \cdot E_{r,i} \qquad \forall i \in I, t \in T. \tag{17}$$

Finally, constraints (18) to (20) ensures the non-negativity of variables,

$$p_{i,t} \geq 0 \qquad \forall i \in I, t \in T, \tag{18}$$

$$e_{in_{i,t}} \geq 0 \qquad \forall i \in I, t \in T, \tag{19}$$

$$e_{out_{i,t}} \geq 0 \qquad \forall i \in I, t \in T. \tag{20}$$

2.2. Real time controller: Power ramp rate limitation

The optimization algorithm previously presented in Section 2.1 solves with the power setpoints for the battery and the supercapacitor for grid power peak shaving purposes. Now, the real time controller presented in this section aims to complement the previous setpoints so the HESS performs also the service of limiting power ramps of the PV plant at its PCC. Power ramp limitation is related to fast and unpredictable power variations of the PV plant, so this controller does not rely on power forecasts but constitutes a responsive, real time decision rule. A graphical description of the real time controller is offered in Figure 3. The input parameters, control setpoints and measurements for the controller are summarized in Table 3. Note that power setpoints $p_{i,t}$ are actually the outputs of the optimization algorithm previously presented in Section 2.1.

The parameters k_1 and k_2 are tuned based on the power ratings and voltage operating range of each of the storage technologies. Thus, for instance, it yields $k_1 = P_{r_1}/(U_{r_1} - U_{min_1})$ for the supercapacitor. The outputs of the real time controller are the setpoints $p^*_{1,t}$ and $p^*_{2,t}$. These setpoints are commanded to the dc-dc converters of the supercapacitor and battery packs, respectively, and include the power needs for both grid peak power shaving and power ramp limitation.

Table 3: Input parameters, control setpoints and measurements for the real time controller

Item	Description
U_1^*	Voltage setpoint for the supercapacitor pack, in V.
U_{r_1}	Rated voltage for the supercapacitor pack, in V.
U_{min_1}	Minimum operating voltage for the supercapacitor, in V.
$u_{1,t}$	Actual voltage of the supercapacitor pack at time t, in V.
$p_{1,t}$	Power setpoint for the supercapacitor pack for peak shaving purposes at time t, in kW.
k_1	Proportional gain for voltage control of the supercapacitor pack.
P_{r_1}	Rated power for the dc-dc converter connected to the supercapacitor pack, in kW.
U_2^*	Voltage setpoint for the battery pack, in V.
U_{r_2}	Rated voltage for the supercapacitor pack, in V.
U_{min_2}	Minimum operating voltage for the supercapacitor, in V.
$u_{2,t}$	Actual voltage of the battery pack at time t, in V.
$p_{2,t}$	Power setpoint for the battery pack for peak shaving purposes at time t, in kW.
k_2	Proportional gain for voltage control of the supercapacitor pack.
P_{r_2}	Rated power for the dc-dc converter connected to the battery pack, in kW.
P_{pv_t}	PV generation at time t, in kW.
n	Number of time steps to consider for power ramp calculation.
μ	Percentage of total power capacity of each storage device to consider for allocating power ramp needs.

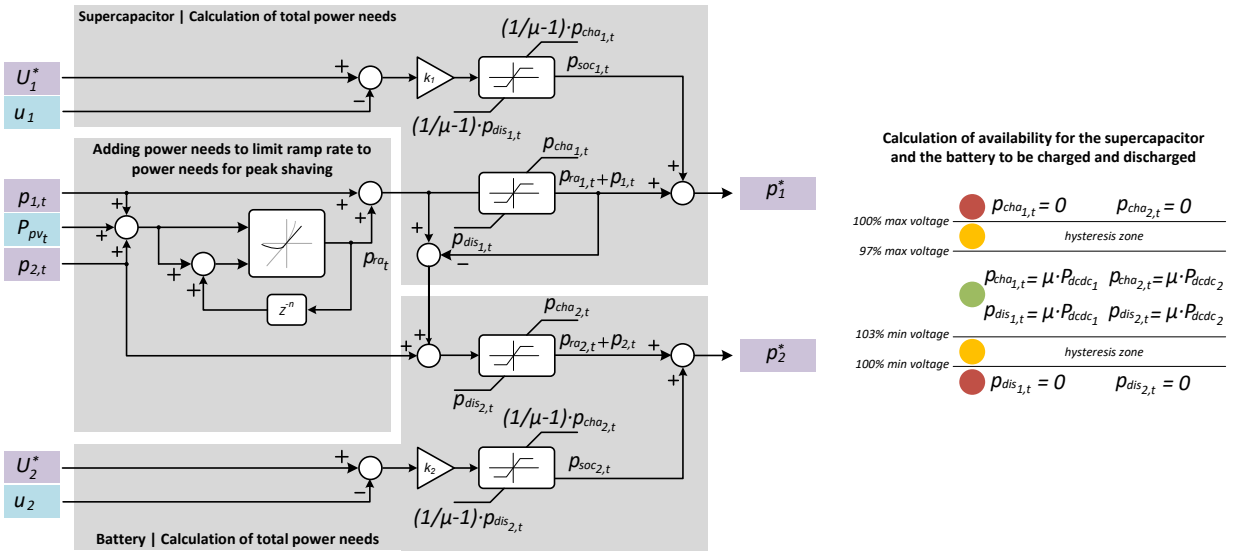

Figure 3: Real time controller for limiting ramp power rates of the PV plant.

As noted in Figure 3, there are three main parts in the algorithm. Firstly, from the measurement of the PV generation, and the power setpoints $p_{1,t}$ and $p_{2,t}$, power ramp limitation needs are calculated (signal P_{ra_t}). Such power ramp needs are primarily associated to the supercapacitor, trying to exploit the fast response and low cycling degradation of this technology. Signal p_{ra_t} is calculated following the guidelines in [31].

The second main block of the real time controller is the named "Supercapacitor | Calculation of total power needs". The output of this block is the final power setpoint to command the dc-dc converter of the supercapacitor, $p^*_{1,t}$. This power setpoint is the sum of a relatively small and slowly varying control signal $p_{soc_{1,t}}$, which is trying to keep the average voltage (or state of charge) of the supercapacitor close to a predefined reference, U^*_1. This control signal $p_{soc_{1,t}}$ complements the signal $p_{ra_{1,t}} + p_{1,t}$, in which $p_{ra_{1,t}}$ corresponds to the power ramp limitation needs previously calculated, p_{ra_t}, but limited by the available capacity of the supercapacitor pack to be charged and discharged (signals $p_{cha_{1,t}}$ and $p_{dis_{1,t}}$) respectively. In case the supercapacitor is not capable of satisfying all power ramp limitation needs, so $|p_{ra_{1,t}}| < |p_{ra_t}|$, the battery is requested to provide the difference among the two signals, being the resultant one of the inputs of the third block of the real time controller.

The third block is mostly analogous to the second one. The final power reference for the dc-dc converter of the battery, signal $p^*_{2,t}$ is the resultant of adding a relatively small and slowly varying power signal trying to keep the average voltage (or SOC) of the battery close to a predefined value U^*_2, and the addition of the power setpoint for PV output ramp limitation to that for grid power peak shaving purposes (so $p_{ra_{2,t}} + p_{2,t}$). It is important to note at this point that in case this exceeds the capacity of the battery to be charged or discharged, part of the ramp limitation needs of the PV plant would not be satisfied.

The last question to complete the description of the real time controller is on how to calculate the capacity of the storage devices to be charged and discharged, so variables $p_{cha_{1,t}}$, $p_{cha_{2,t}}$, $p_{dis_{1,t}}$ and $p_{dis_{2,t}}$. This explanation is supported by the right picture in Figure 3. As shown, such capacity is voltage dependant. In case the voltage of the storage devices is within admissible limits, i.e. not exceeding 97% of the maximum value and holding more than 103% of the minimum operating level, the capacity mainly corresponds to the ratings of the attached dc-dc converters, so P_{r_1} and P_{r_2}, but just substracting a small percentage $(1 - \mu)$, allocated for average state of charge correction, as noted before. Conversely, if the voltage of the storage devices is out of the thresholds, no power setpoint is solved for PV power ramp rate limitation neither for grid power peak shaving purposes. In other words, $p_{cha_{1,t}}$ or $p_{cha_{2,t}}$ are set to 0 to avoid overcharge; or

$p_{dis_{1,t}}$ or $p_{dis_{2,t}}$ are set to zero to avoid excessive discharge. Two hysteresis zones separate the "green" or safe voltage operating range to the prohibited (or "red") one for stability. That is, a transition from the green to the red zone implies a linear decrement of charge and discharge capabilites throughout the orange zone, so $p_{cha_{1,t}}$ and $p_{dis_{1,t}}$ for the supercapacitor (and analogously for the battery). Further, and for the case of the supercapacitor –the same applies to the battery–, charge and discharge capacities, so $p_{cha_{1,t}}$ and $p_{dis_{1,t}}$, are set to zero till the voltage is corrected enough to recover the safe or green operating range again.

3. Case study - A PV plant connected to a distribution grid

The main objective of this case study is to evaluate the performance of the optimization algorithm (i.e. the highest level of the PV plant controller) for grid power peak shaving. The second objective is to also evaluate the performance of the HESS in keeping PV plant power ramp within permitted thresholds.

3.1. Selection of grid, PV plant and HESS characteristics

This case study adopts real world data for a 9.4 MW PV plant [31]. The corresponding generation time profile is scaled down to represent a 6.6 MW PV plant and it is connected to a distribution grid with 6 MVA rated power. All in all configures an scenario in which the renewable generation even exceeds in 10% the ratings of the grid. Without no management on active –and reactive– power exchange, the PV plant would provoke excessive overvoltage at its PCC, so the selected case study properly fits with the objectives of the paper. Figure 4 depicts the weekly PV generation profile, highlighting the weekly cumulated generation and the average daily estimation. Further characterizing the case study, the nominal grid voltage is $E = 3.3$ kV, the short-circuit impedance is 10%, yielding a grid short-circuit resistance of $R = 0.0726$ Ohm and short-circuit reactance $X = 0.1663$ Ohm.

The average daily PV generation, along with the time-dependent profile in Figure 4, are considered as main input parameters for selecting the power and energy storage requirements of the lead-acid battery and supercapacitor packs embedded into the HESS. Power requirements are associated to PV output peak shaving needs. The peak value of 6.6 MW should be diminished down to 6 MW (so 10% reduction), at least, to not provoke excessive grid overvoltage. Extending this margin to 20%, this yields 1.32 MW in power. This should be the minimum rating of the lead-acid and supercapacitor packs, and thus of the corresponding dc-dc converters. However, and as explained in Section 2.2, the lead-acid battery pack should ensure a proper response of the HESS for PV plant power ramp limitation even at the eventuality of exhausting the capacity of the supercapacitor. For this reason, the rated power of the lead-acid battery pack is doubled to 2.64 MW.

Most of the energy storage capacity of the HESS is provided by the lead-acid battery, since offering much higher energy density than supercapacitors. The energy storage capacity of the lead-acid pack can be selected as a fraction of the average daily PV output (26.8 MWh, see Figure 4). According to the time-dependent PV generation profile, the HESS should alleviate grid power injection by the PV plant for a period of less than 2 hours in days with high solar irradiation. Thus, considering that the lead-acid battery pack would provide most of this energy and working at rated power in the most challenging case, it yields a energy storage capacity of 2.64 MW times 2 hours, so 5.28 MWh. A total capacity of 5.5 MWh is finally selected in this case.

The last metric to determine about power and energy storage capacities is the rated energy of the supercapacitor pack. The function of the supercapacitor is to mostly limit power ramps of the PV plant at its PCC. According to the EU Commission Regulation 2016/31 [30], the power ramp of the output of the plant should not overcome a threshold value expressed in MW/second, that in the present case study is set at 0.1 MW for a 10-second period. The energy involved in such power variation is relatively reduced, and this makes supercapacitors as well suited option for this service. In the HESS though, the supercapacitor is also participating in the service of PV output peak shaving, and according to the design of the optimization algorithm for the HESS schedule in Section 2.1, it means to fulfil power requests for 15-minutes period. From the considerations above, the rated energy storage capacity of the supercapacitor pack is set to 0.25 MWh. Setting this, the supercapacitor pack would be able to follow power setpoints of hundreds of kW for 15-minutes period, thus making it practical for peak shaving purposes and in addition slightly alleviating the stress of the lead-acid pack.

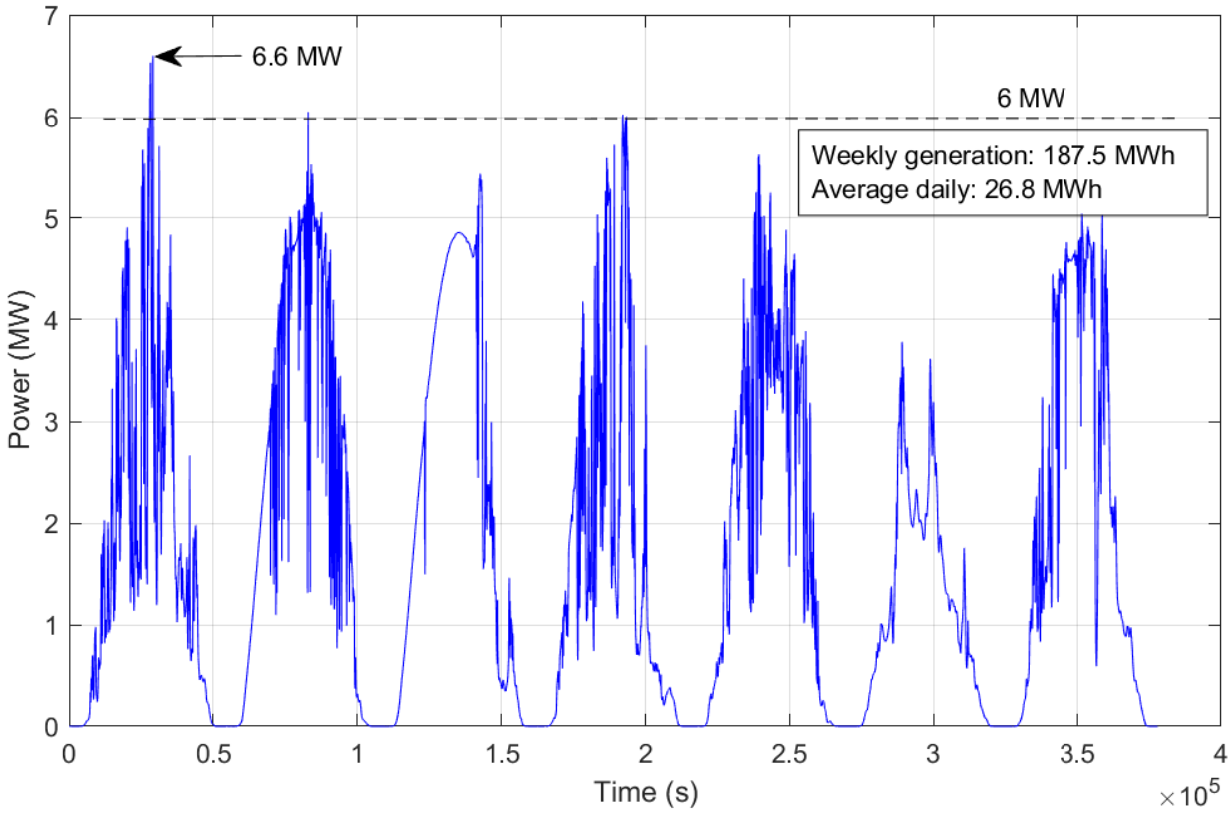

Figure 4: Weekly PV generation profile. Grid ratings are noted by a dashed line at the level of 6 MW.

So to sum up, the ratings of the supercapacitor pack are $E_{r_1} = 0.25$ MWh and $P_{r_1} = 1.32$ MW. The lead-acid battery pack doubles the power capacity of the supercapacitor pack reaching $P_{r_2} = 2.64$ MW and it hosts 22 times the energy storage capacity of the supercapacitor pack as well, so $E_{r_2} = 5.5$ MWh. In terms of power, the supercapacitor is rated at 20% of the nominal power of the PV plant and the battery pack is rated at 40% of the nominal power of the PV plant. Finally, it is important to note that practical energy storage capacities will be diminished in the following, from the considered state of charge operating regimes.

The procedure to determine the number of supercapacitor modules connected in series and in parallel to configure a pack rated at $E_{r_1} = 0.25$ MWh and $P_{r_1} = 1.32$ MW is explained in the following. First, a supercapacitor module is selected from the market. The reference BMOD0141P064B04 from Maxwell Technologies [32] is selected in this case, since being suitable to configure packs reaching high voltage and thus high power, e.g. in the range of 1000 and 2000 V. The rated voltage per module is 64 V and the capacitance is 141 F. To avoid excessive overvoltage at high state of charge, and excessive currents through the pack and low state of charge, the state of charge operating range is limited between 0.95 and 0.25 p.u. By setting 34 modules in series and 92 strings in parallel the rated energy of the pack is 0.25 MWh. The rated voltage of the pack is $U_{r_1} = 2156$ V, the voltage at state of charge 0.95 p.u. is 2101 V, and the voltage at state of charge 0.25 p.u. is $U_{min_1} = 1010$ V. Adopting the above mentioned state of charge operating range, the practical energy provided by the pack is 0.17 MWh, which is considered an admissible value for the purposes of the work. Further, at minimum operating voltage, at the circumstance of exchanging the rated power, the total current exchanged with the dc-dc converter is 1307 A, which is considered an admissible value for commercial transistors (IGBTs) building up power converters in the MW-range.

Analogously, the procedure to determine the number of batteries connected in series and in parallel to configure a pack rated at $E_{r_2} = 5.5$ MWh and $P_{r_2} = 2.64$ MW is explained in the following. First, a battery model is selected from the market. The reference UCG75-12 from Ultracell [33] is selected in this case, since considered suitable to scale up to the ratings of the pack. The rated voltage of the battery is 12 V and its capacitance is 75 Ah at C10. To avoid excessive overvoltage at high state of charge, and to protect the pack from excessive depth of discharge, the state of charge operating range is limited between 0.95 and 0.25 p.u. By setting 169 modules in series and 36 strings in parallel the rated energy of the pack is 5.48 MWh. The rated voltage of the pack is $U_{r_2} = 2270$ V, the voltage at state of charge 0.95 p.u. is 2215 V, and the voltage at state of charge 0.25 p.u. is $U_{min_2} = 2008$ V. Adopting the above mentioned state of charge operating range, the practical energy provided by the pack is 3.83 MWh, which is considered an admissible value for the purposes of the work. Further, at minimum operating voltage, at the circumstance of exchanging the rated power, the total current exchanged with the dc-dc converter is 1314 A, which is considered an admissible value for commercial transistors (IGBTs) building up power converters in the MW-range.

3.2. Obtained results

This sections presents the performance of the 2-level PV plant controller, i.e, the optimization algorithm for grid power peak shaving and the real-time controller for PV plant power ramp limitation. Firstly addressing the grid power peak shaving service, the following state of charge limitations are adopted for the supercapacitor (sub-index 1) and the lead-acid battery packs (sub-index 2): $SOC_{max_1} = 0.7$ p.u., $SOC_{max_2} = 0.95$ p.u., $SOC_{min_1} = 0.50$ p.u., $SOC_{min_2} = 0.25$ p.u. As noted, the whole admissible operating range for the lead-acid battery is envisaged here, since this storage device is the main contributor in grid power peak shaving service. For the supercapacitor though, just a limited operating range is allocated, since its contribution in this service is just complementary to the lead-acid battery pack. The initial state of charge of the superacapacitor pack is set at the mid point of its state of charge operating range, so at 0.6 p.u. The initial state of charge of the battery pack is set at 0.45 p.u., thus also yielding the optimization algorithm freedom to charge and discharge the battery from the very beginning of the optimization time horizon, which comprises 96 periods of 15 minutes each (so 24 hours).

Figure 5 summarizes the results of the optimization algorithm, i.e. the highest level of the PV plant controller aiming to perform grid power shaving. The upper-left subplot compares the PV generation profile (grey line, thus representing the case in which no power management is performed), with the net active and reactive power scheduled by the optimization problem (solid and dashed blue lines, respectively). As can be

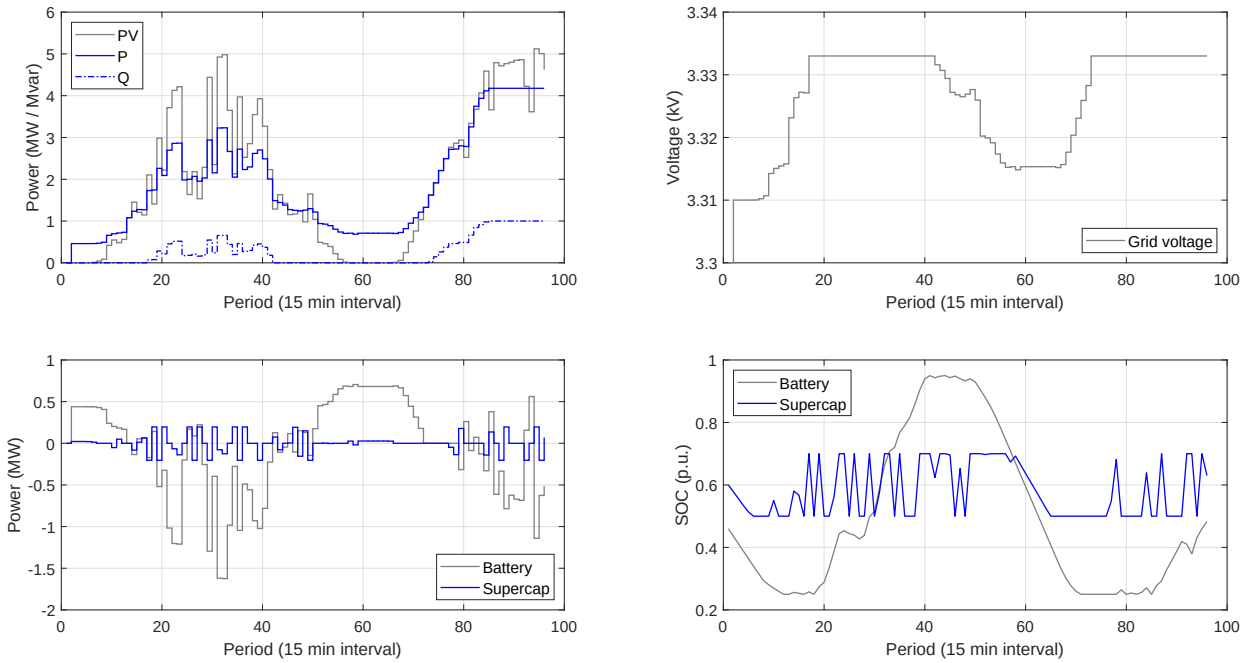

Figure 5: Results of the optimization algorithm, addressing the power management of a large PV plant exceeding the ratings of the grid.

noted, the peak active power exchanged by the PV plant with the contribution of the HESS results clearly diminished. As a result of this active and reactive power management, and as noted in the upper-right subplot, the voltage level at the PCC is limited to its maximum thereshold, which is around 3.333 kV, so 1% overvoltage.

The bottom-left and bottom-right subplots then concentrates on the actuation of the battery and the supercapacitor. As noted, the supercapacitor is continuously being charged and discharged, as its energy storage capacity is rapidly exhausted. Conversely, the battery just performs approximately one cycle during the 96 periods of 15 minutes that lasts the optimization (so 24 hours), and this promotes a larger lifespan for this storage device.

For the real-time controller for PV plant power ramp limitation, the following state of charge limitations are adopted for the supercapacitor (sub-index 1) and the lead-acid battery packs (sub-index 2): $SOC_{max_1} = 0.7$ p.u., $SOC_{max_2} = 0.95$ p.u., $SOC_{min_1} = 0.25$ p.u., $SOC_{min_2} = 0.95$ p.u. These limitations are translated into the real-time controller into voltage limits, as previously explained in Section 2.2 and graphically depicted in Figure 3. Results in the following thus show the performance of the whole PV plant controller, including the services of grid power shaving and power ramp limitation.

Figure 6, upper subplot, compares the PV generation (grey line) with the final active power exchanged by the PV plant, including the hybrid storage solution. The first comment here is that now signals are much more variable, compared to the results in Figure 5, since not discretized with a time step 15 minutes, being this how these are treated for the optimization problem. Because of the variability in sun irradiation, and evaluating the grey line, it is clear that eventually, the PV generation exceeds 6 MW, which is the rated power of the grid. Despite of this variability, the PV plant controller manages to reduce peak power exchange. This can be better observed in the subplots at the bottom. The one at the left compares the actual output of the plant with the ratings of the grid (noted by the quarter-circle represented with a solid black line). The box-plot in the right, further emphasises in the reduced variability and maximum magnitude of the developed apparent power thanks to the contribution of the hybrid energy storage solution.

Results in Figure 7 depict how power ramp of the output of the PV plant results perfectly limited to

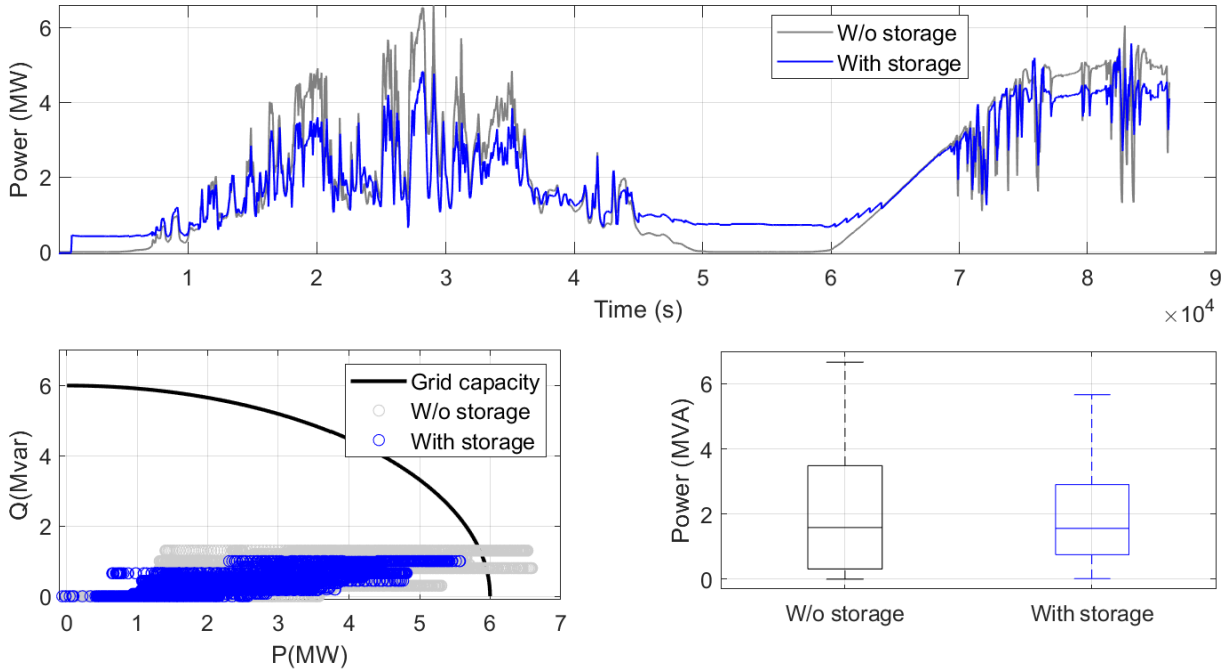

Figure 6: Performance of the 2-level PV plant controller in limiting the peak power exchanged with the grid.

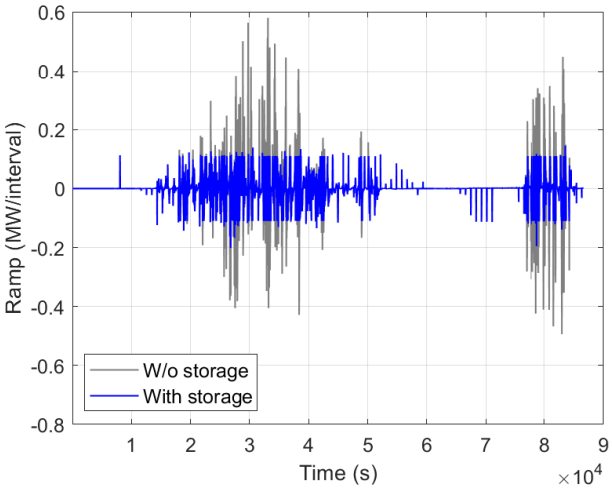

Figure 7: Performance of the 2-level PV plant controller in limiting the power ramp rates.

the maximum threshold, which is about 0.1 MW for a 10 second period. Such power ramp limitation is mostly thanks to the fast and continuous cycling of the supercapacitor, as noted in Figure 8, upper-left subplot. The upper-right subplot depicts the state of charge of the two storage technologies. As can be clearly observed, both technologies reach the predefined limits, i.e. 0.25 p.u. and 0.95 p.u. state of charge.

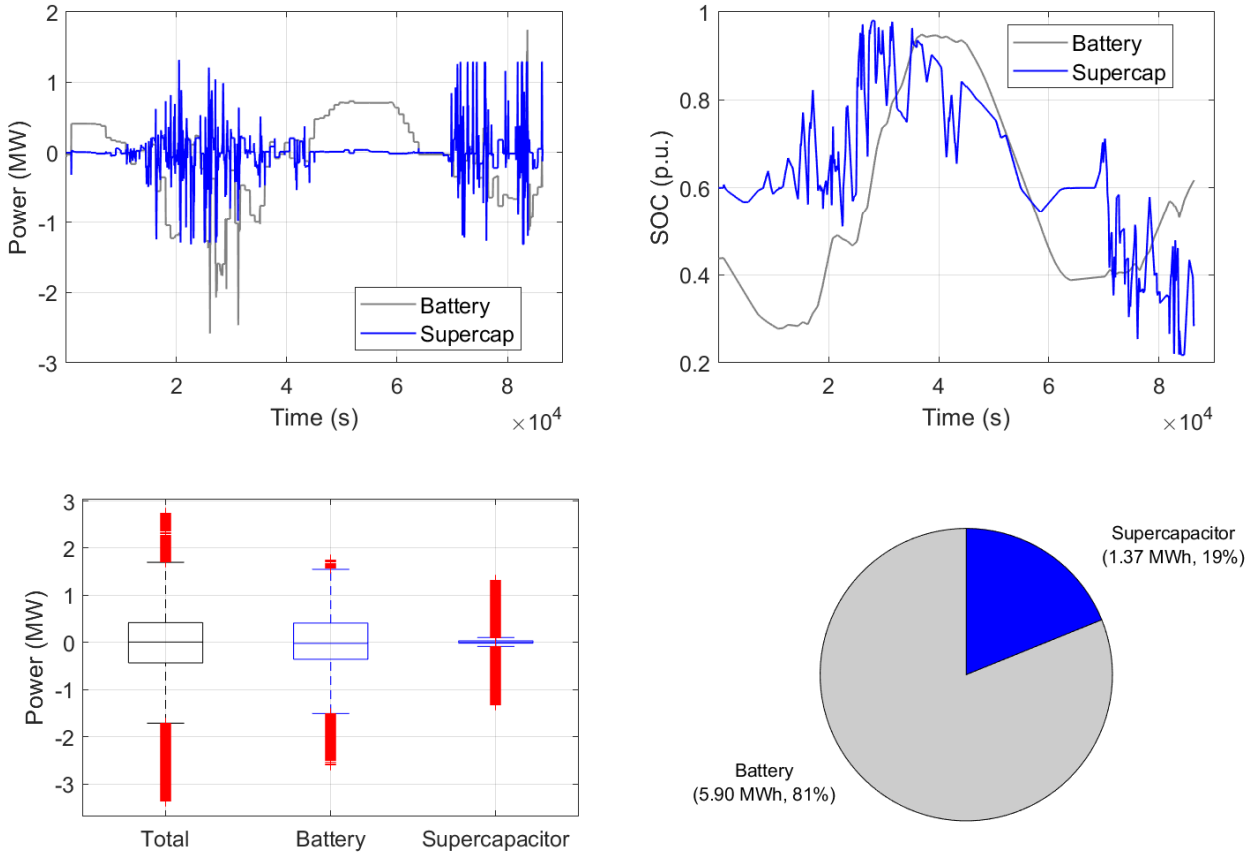

Figure 8: Performance of the 2-level PV plant controller in limiting the peak power exchanged with the grid.

The time-dependent power profile and state of charge of the supercapacitor and the battery clearly highlight the advantage of hybridizing the storage solution over conventional approaches based on just one technology: the lead-acid battery pack is providing a sustained power for prolonged periods of time, while the supercapacitor pack is being continuously cycled for PV plant power ramp limitation. The actuation of the supercapacitor pack reduces the battery pack stress, thus extending its lifespan. Supporting such synergistic operation, the two lower subplots in Figure 8 offer quantifiers on power and energy distribution. In terms of power, the box plot for the battery pack depicts that the first and third quartile of analyzed data are located at -0.35 MW and 0.41 MW respectively. Bearing in mind that the rated power for the battery pack is 2.64 MW, the usual power stress the battery is subjected to is within 13.2% and 15.5% of the rated power. The shape of the box plot for the supercapacitor is qualitatively and quantitatively different than for the battery pack. First, the areas determining the first and third quartile are very close, thus yielding the idea that the power developed by the supercapacitor is reduced most of the time. However, the important presence of outliers is associated the reactive and abrupt response of the supercapacitor pack to eventually limit the PV power ramp rate. Further analysing the synergistic operation of the two storage devices, the pie graph in Figure 8 now compares the total energy discharged. As shown, 18.1% of total energy injected to the grid by the HESS is provided by the supercapacitor. Again, this is energy not provided by the battery, thus resulting into an extended lifetime of this storage device.

4. Experimental validation

The case study in Section 3 focused on the performance of the HESS for the provision of services to a large scale PV plant. Results depict the correctness and performance of the 2-level PV plant controller while simultaneously managing the lead-acid battery and supercapacitor packs. Complementary, the validation described in this section, based on a lab-scale prototype of the HESS, emphasizes on the performance of the algorithms in sharing the power demand among the lead-acid and the supercapacitor packs. Experiments cover operational circumstances as reaching the operational limitations (e.g. voltage threshold levels) for the storage technologies to check the correctness of the control algorithms in there.

4.1. Selection of grid, PV plant and HESS characteristics

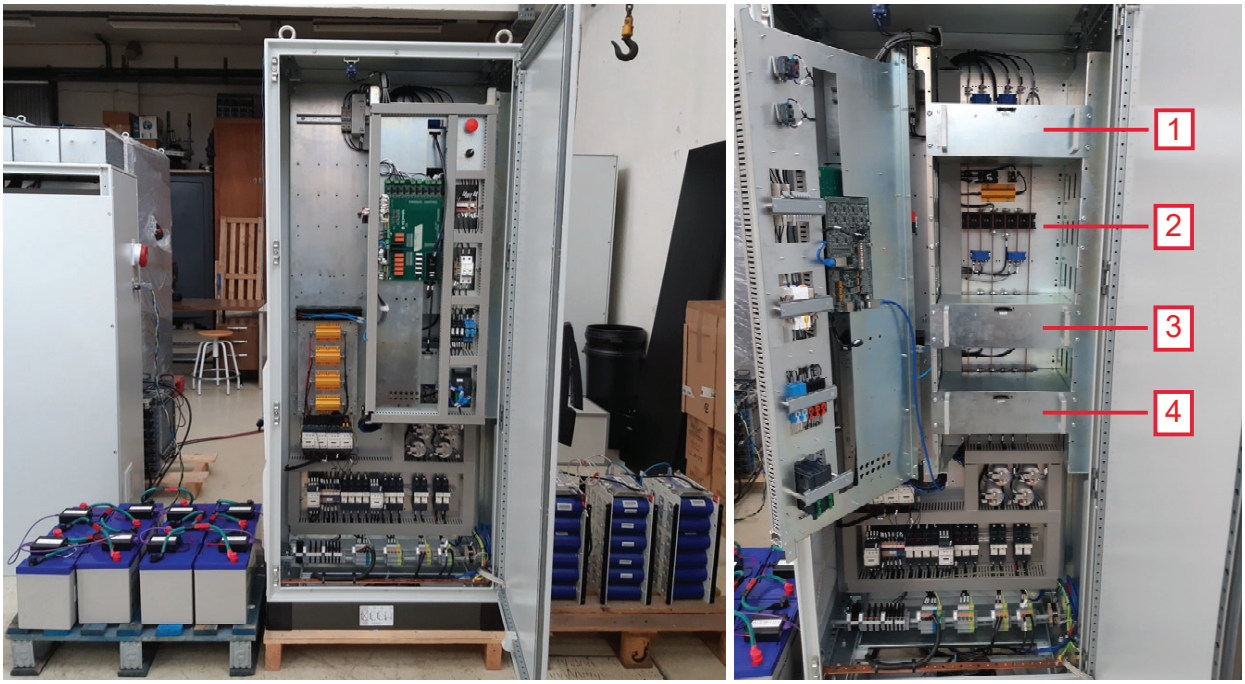

Figure 9: Lab-scale prototype for the hybrid energy storage solution. Label 1 indicates the grid inverter. Label 2 corresponds to the common dc-link at which dc-dc converters 3 and 4 are connected to.

The lab-scale prototype is shown in Figure 9. As can be observed, the core technology for the HESS solution is a power electronics cabinet including dedicated dc-dc modules for the integration of the lead-acid and the supercapacitor packs. The rated energy of the supercapacitor and lead-acid battery packs are coherently selected to the ones determined for the grid-scale case study in the previous Section 3. Also, the model for the battery and the supercapacitor module to be considered here are the same in the previous Section 3 for consistency.

While the rated energy of the supercapacitor pack in Section 3 was set to 0.25 MWh, for the lab-scale prototype it is 0.25 kWh. Three modules from Maxwell Technologies, reference BMOD0141P064B04 [32], are connected in series, thus yielding a maximum voltage of $U_{max_1} = 192$ V. By setting the minimum operating state of charge to 0.25 p.u., the minimum voltage results as $U_{min_1} = 89$ V. Analogously, while the rated energy of the battery pack in Section 3 was set to 5.5 MWh, for the lab-scale prototype it is 5.5 kWh. The pack is composed by 8 batteries in series, reference UCG75-12 from Ultracell [33], thus yielding a maximum voltage of $U_{max_2} = 116$ V. By setting the minimum operating state of charge to 0.25 p.u., the minimum voltage results as $U_{min_2} = 95$ V.

The peak power of the PV plant to consider now is 6.6 kW and the maximum power to be exchanged with the grid is 6 kVA. The corresponding time-dependent power profile is built by scaling down the profile considered in Section 3, for consistency. Also for consistency, the maximum power the supercapacitor pack can develop is limited to 20% of the ratings of the PV plant, so 1.32 kW; and the maximum power the battery pack can develop is set at 40% of the ratings of the PV plant, so 2.64 kW. As discussed, the rated power of the battery pack (and thus of the associated dc-dc converter) should be higher than for the supercapacitor, so the battery pack can react in case of exhausting the limited storage capacity of the supercapacitor.

4.2. Obtained results

As for the analyses in Section 3, for the optimization algorithm solving the provision of grid power peak shaving, the following state of charge limitations are adopted for the supercapacitor (sub-index 1) and the lead-acid battery packs (sub-index 2): $SOC_{max_1} = 0.7$ p.u., $SOC_{max_2} = 0.95$ p.u., $SOC_{min_1} = 0.50$ p.u., $SOC_{min_2} = 0.25$ p.u. The initial state of charge of the superacapacitor pack is set at the mid point of its state of charge operating range, so at 0.6 p.u. The initial state of charge of the battery pack is set at 0.45 p.u., thus also yielding the optimization algorithm freedom to charge and discharge the battery from the very beginning of the optimization time horizon (86400 seconds, so 24 hours).

The first results shown in Figure 10, are consistent with those obtained in in Section 3. As shown, the peak power exchanged with the network is effectively reduced, thus leaving maximum values below 6 kW. In terms of apparent power, values are below the maximum thereshold imposed by grid ratings. Such power limitation is thanks to the combined actuation of the battery and supercapacitor packs. The subplot in the second row in Figure 10 clearly depicts that the power profile developed by the supercapacitor is much more volatile than that for the battery pack, and this is because the supercapacitor is taking over most of power ramp limitation needs, while the sustained provision of power by the battery is to shave the peak power exchanged with the network. The aprupt response of the supercapacitor can be further observed by the large quantity of outliers in the box plot graphic. The synergistic operation of the two storage technologies embedded into the hybrid solution, permits to reduce the total battery output (15% of total energy provided by the hybrid solution is through the supercapacitor pack), thus extending its lifespan.

Figure 11 offers a closer look at the operation of the supercapacitor pack. The upper subplot highlights again its stochastic and aprupt operation, mostly governed by the output of the real time controller for PV power ramp limitation purposes. The power reference profile is the resultant of the combination of a time dependant power profile with 15-minutes time step, and the stochastic and abrupt output of the real time controller. As can be observed, the maximum power is not exceeding the ratings of this device, which are limited at 1.32 kW. The second subplot depicts the voltage profile. The maximum and minimum voltage thereshold values are noted by the red lines. The green lines limit the operational zones at which the maximum power can be developed by the device, as there is no risk of excessive over and undervoltage (the reader is referred to Section 11 for a detailed explanation of these voltage limits, included in the real time controller). To keep a constant average state of charge –and thus an average voltage–, the real time controller included the parameter μ. This is a value between 0 and 1, weighting the portion of the total power capacity of the storage technologies saved for this purpose. From the beginning of the experiment and till almost reaching 70000 seconds, μ was set to 0.99. This value, for the supercapacitor, means that self-discharge losses can be compensated by developing a maximum power of $(1-\mu)\cdot P_{r_1}$, so $(1-0.99)\cdot 1.32 = 0.013$ kW (13 W). The sustained decrement in the voltage of the supercapacitor clearly depicts that this power capacity is not enough to compensate self-discharge phenomena. The application of $\mu = 0.97$ (so increasing the available power for this purpose to 40 W) rapidly corrects this voltage decrement, keeping it within admissible limits again. This experiment serves to validate the control loop included in the real time controller for self-discharge phenomena correction. Finally, there is a zone squared in Figure 11 that serves to test the synergistic operation between the supercapacitor and the battery in case of exhausting the supercapacitor energy storage capacity. This will be explained later in the section, while tackling a closer view to the battery pack behavior.

Figure 12 addresses the operation of the battery pack. The first subplot clearly depicts that the power is mostly commanded by 15-minutes time step profile, so the output of the optimization algorithm for PV plant peak power shaving purposes. There are few aprupt peaks, associated to the circumstances the battery

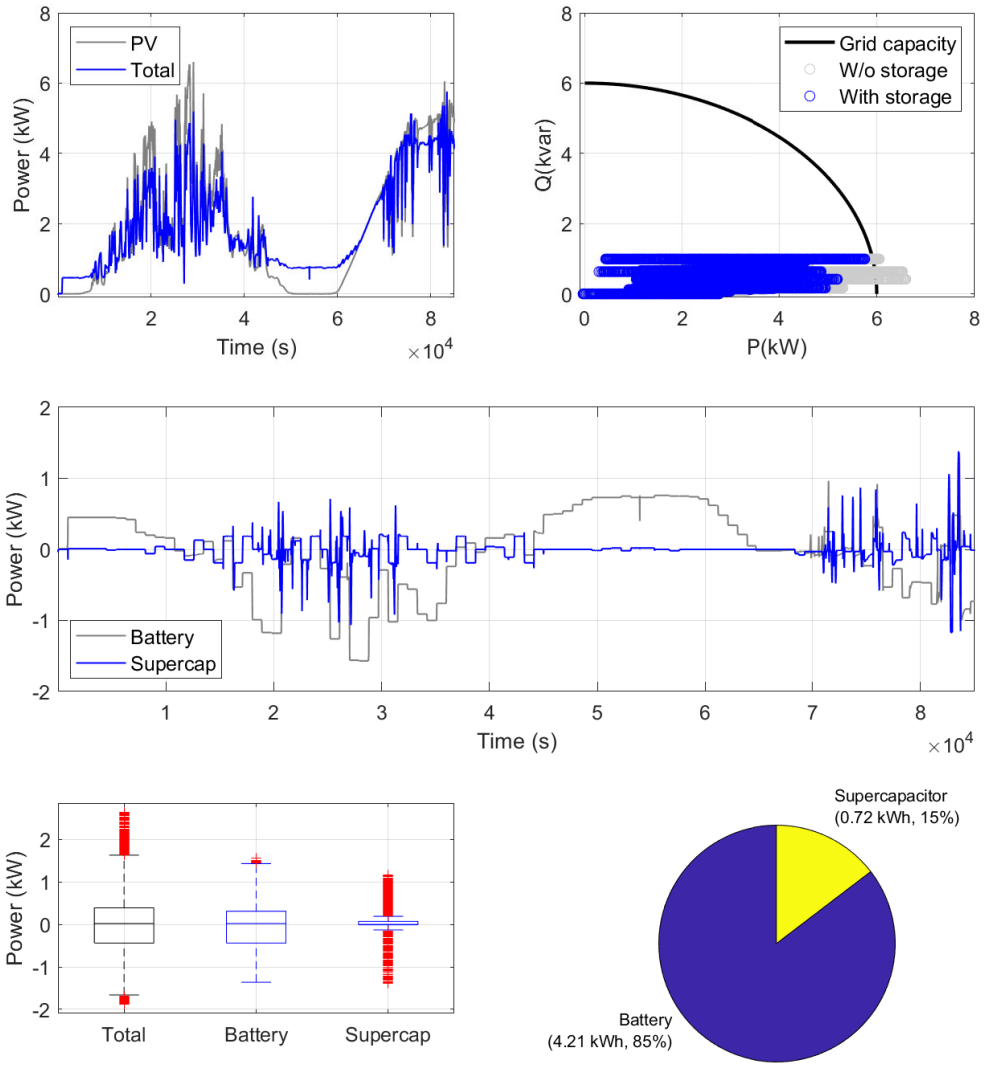

Figure 10: Experimental results. The first row plots the total output of the PV plant with and without the contribution of the hybrid energy storage solution; the second row shows the active power profiles for the battery and supercapacitor packs; and the third row quantifies the contribution of each storage technology in terms of power and energy.

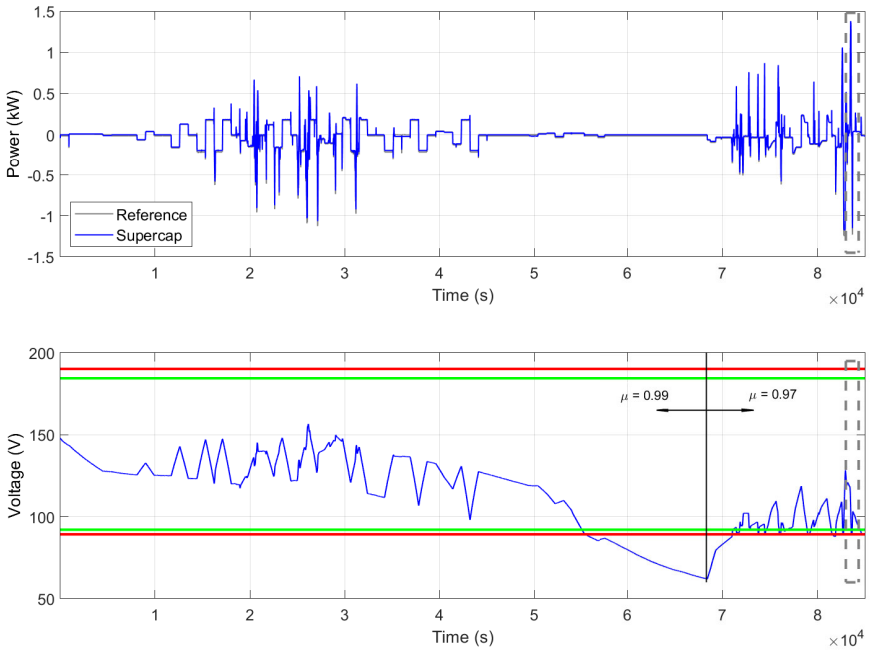

Figure 11: Experimental results. Operation of the supercapacitor pack. The first subplot shows the power developed and the corresponding setpoint; the second subplot depicts the voltage profile and corresponding thereshold levels.

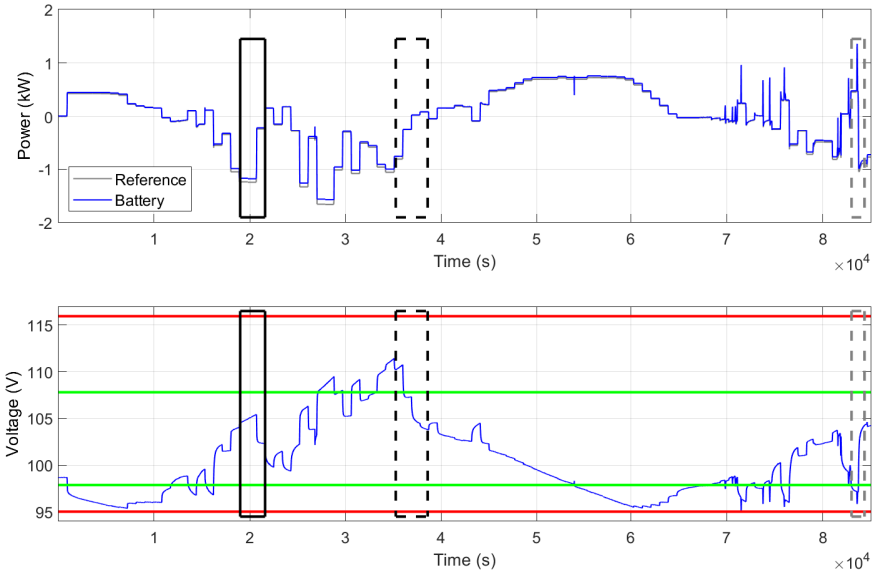

Figure 12: Experimental results. Operation of the battery pack. The first subplot shows the power profile and the corresponding setpoint; the second subplot shows the voltage profile and corresponding thereshold levels. The black solid squared zone is named Zoom A. The black dashed squared zone is named Zoom B. The grey dashed squared zone is named Zoom C.

takes the lead in providing the service of PV plant power ramp limitation. These peaks are frequent in the last part of the experiment and this is because, as noted before, the voltage of the supercapacitor pack was very limited and thus it has not enough energy to satisfy all power ramp needs. The second subplot shows how the voltage increases and decreases according to the charge and discharge processes, and thus to the state of charge. One important difference with supercapacitors is that now the histeresis zone for the real time controller (so the voltage range between the red and green lines in Figure 12) is remarkably wider. This is because the battery pack experiences important over and undervoltage while being charge and discharge due to its internal resistance and also because of the non linear shape for its open circuit voltage characteristic, specially while reaching the maximum and minimum state of charge levels. So it may happen that the battery has a voltage close to its maximum value but still in the normal operating zone (so below the green line), but this voltage rapidly increases as soon as exchanging power, and it can even potentially reach the maximum admissible value (noted by the upper the red line). To protect the battery pack from excessive overvoltage, the zone at which it can develop the rated power (zone limited by the two green lines) is much more limited than for supercapacitors. This is a clear advantage of supercapacitors over lead-acid batteries: the possibility of developing large power even while close to the maximum and minimum state of charge levels.

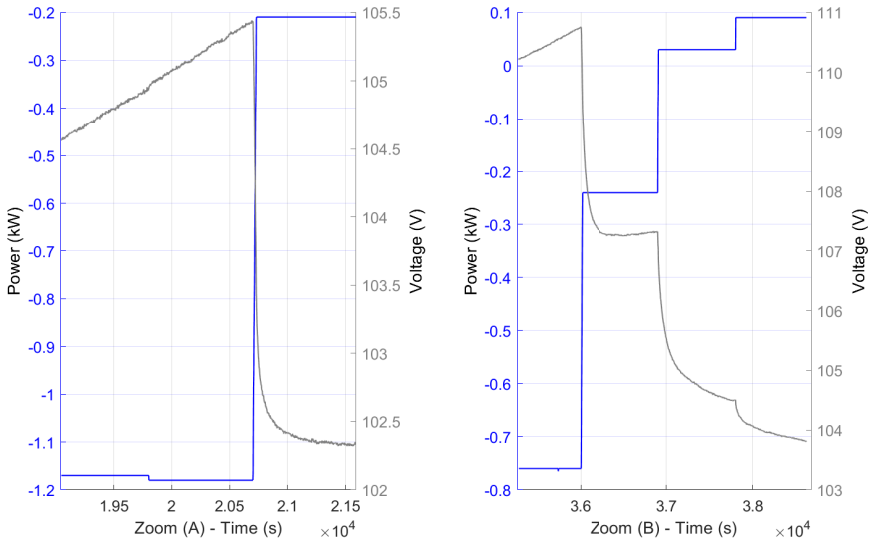

Figure 13: Experimental results. Zone named as Zoom B, highlighting the overvoltage of the battery pack because of the power exchanged.

This important overvoltage the battery experiences at the circumstance of exchanging power due to its internal resistance can be evaluated in the solid and dashed squared black zones in Figure 12, which are zoomed in Figure 13, for the sake of clarity. The subplot in the left presents the Zoom A. The battery is being charged at 1.18 kW and the voltage is increasing accordingly. As soon as diminishing the power exchanged down to 0.2 kW, there is a voltage drop of about 3 V. Similarly, in the Zoom B, it can be noted how the overvoltage in the battery decreases with the power developed. Such important voltage variability with the power developed –and not necessarily with the state of charge– is an operational constraint for lead-acid batteries, specially in applications in which there is a recurrent cycling and stringent power stress level. The hybridization is considered here as an added value over solutions just based on lead-acid batteries.

The real time controller for PV power ramp rate limitation progressively reduces the power capacity of the lead-acid battery –and of the supercapacitor pack– in the hysteresis zone (so in the zone limited by green and red lines in Figure 12). To evaluate such power capacity decrement, the results of a simple test in which the a step profiled power setpoint of 1.6 kW (charge power) is commanded to the battery, see Figure 14. As noted, at the beginning of the experiment, the battery was almost in rest conditions

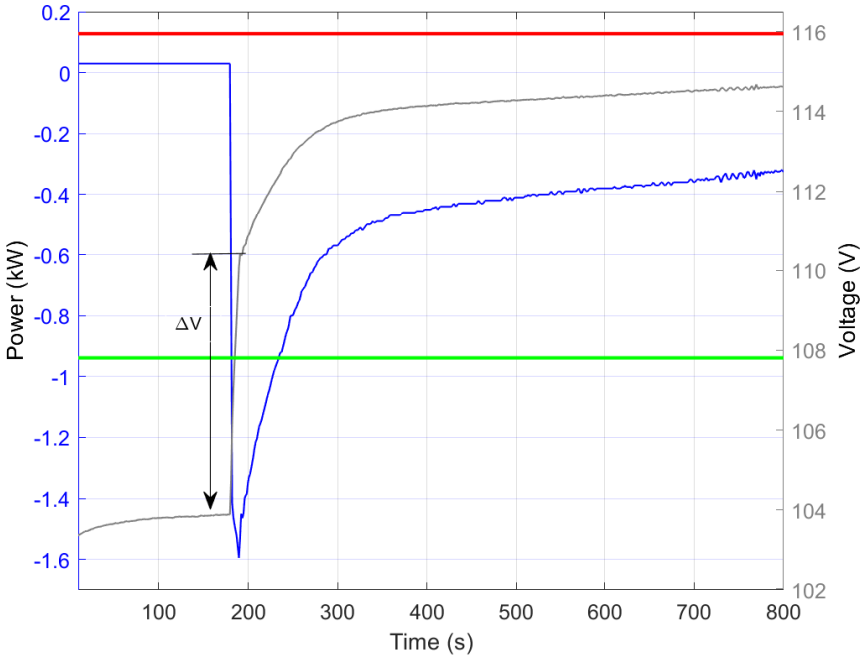

Figure 14: Simple experiment showing the instantaneous overvoltage due to the internal resistance, and the decremental power capacity of the battery governed by the real time controller, as the voltage aproaches the maximum admissible level.

(the power developed is almost zero), and at time 190 s, it receives a power command of 1.6 kW. Due to the internal resistance, there is an instantaneous overvoltage of about 6 V that makes the voltage of the battery pack to remain within the hysteresis zone. In this zone, and while the battery is being charged, the power developed is limited by the real time controller according to the voltage increment. As the voltage gets closer to the maximum thereshold, the power that can be developed is reduced. This controller avoids excessive instantaneous overvoltages within the hysteresis zone that may led the voltage of the battery out of admissible levels.

Going back to the experiment in Figure 11 and Figure 12, a final closer look in provided, now addressing the dashed grey squared zone, Zoom C. Figure 15 represents in a single graph the power developed by the battery and the supercapacitor packs, and the voltage of the supercapacitor in this Zoom C. As noted, the voltage of the supercapacitor is decreasing till time $8.36{\cdot}10^4$ s, because the supercapacitor is being discharged (is developing a positive power). At the above mentioned time, the voltage reaches the minimum admissible value, 89 V, so the battery pack is replacing the supercapacitor for PV power ramp rate purposes. This is a clear example on the synergistic operation of the two storage devices at the circumstance of exhausting the energy storage capacity of one of them and thus ensuring a proper service level from the hybrid solution to the PV plant.

5. Conclusions

In this work, a PV plant controller for a HESS to provide the services of PV power peak shaving and power ramp limitation has been effectively developed and validated. The main conclusions of the work are:

- The 2-level architecture of the PV plant controller has been proved effective to manage the power requirements from a HESS for the provision of two complementary services for the grid integration of the PV plant. These two services, in fact, address the needs of two agents: the PV plant operator and the DSO. The PV plant operator is benefited from the operation of the HESS by fulfilling grid code

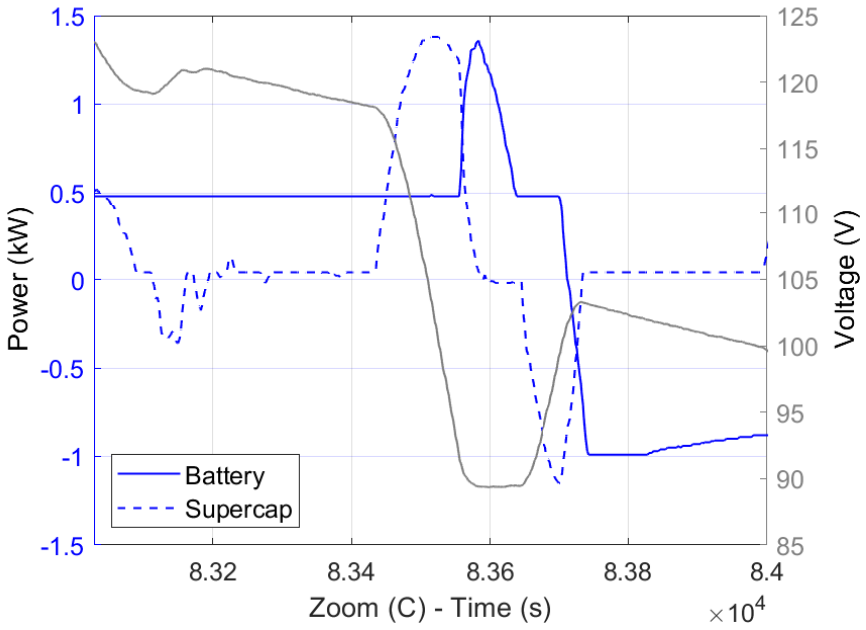

Figure 15: Experimental results. Zone named as Zoom C, for evaluating the synergistic operation of the supercapacitor and battery packs.

requirements. The DSO is benefited by avoiding grid overvoltages, thus potentially deferring in time new investments for grid reinforcement.

- The service peak power shaving required the exchange of remarkable energy from the HESS, while the service of power ramp limitation required a fast and reactive response addressing PV output stochastic profile. The hybridization of the storage system, based on the combination and synergistic exploitation of a lead-acid battery and a supercapacitor pack, has been proved effective to cope with such variety of technical requirements.

- The optimization algorithm along with the real time controller permitted to exploit the complementarity of the two storage technologies. According to the simulation and experimental results obtained in this paper, the total energy discharged by the lead acid battery pack was reduced between 15% and 19%, thanks to the contribution of the supercapacitor pack. Also, the power stress for the battery pack was limited within 13.2% and 15.5% of its rated capacity since most of fast response requirements were associated to the supercapacitor pack. This synergistic operation favors an extended battery life.

- The lead-acid battery pack was proved effective in providing a sustained power for PV peak power shaving purposes, and also to limit the power ramp rate at the circumstance of exhausting the energy storage capacity of the supercapacitor. However, two important aspects should be taken into account for a proper integration and operation of the lead-acid battery pack in the HESS: i) the power ratings of the lead-acid battery pack should be higher than for the supercapacitor pack so the battery pack can react in case of exhausting the limited storage capacity of the supercapacitor (in the present paper, the battery pack was rated at 40% of the ratings of the PV plant, and the supercapacitor was rated at 20% of the PV plant ratings); ii) The voltage window at which the battery can be operated at full power should be narrowed so as to avoid excessive overvoltage while being charged and discharge close to its maximum and minimum state of charge levels.

From the conclusions derived from the present work and as further research, the authors identify the convenience to apply advanced modelling techniques for the lead-acid battery pack that permit to reliably

represent the behaviour and performance of this storage technology especially at the circumstance of reaching maximum and minimum state of charge levels. As noted in the project, the exponential variation of the voltage of this battery type when reaching above mentioned state of charge limits importantly bound the power capacity and this may affect the service level offered by the whole HESS. Techniques employed for lithium-ion batteries as the mapping of the available power with respect to the state of charge level (i.e. the so-called State of Available Power, SoAP metric) would enhance the power scheduling of the lead-acid battery. In addition, the application of machine learning techniques as, for instance, Kalman filters, would permit to reliably represent the behaviour and state of the battery (e.g. by recurrently updating the value of its efficiency and state of charge).

6. Appendix

The common parameters for the case study involving a large scale PV plant connected to a weak distribution grid (see Section 3) and for the experimental validation (see Section 4), all in correspondence with the codification in Tables 1 and 3 are: $T = \{1, .., 96\}$, $I = \{1, 2\}$, $T_s = 0.25$ h, $\varepsilon = 0.05$ p.u., $\eta_{in_1} = 0.98$ p.u. (supercapacitor), $\eta_{in_2} = 0.91$ p.u. (battery), $\eta_{out_1} = 0.98$ p.u. (supercapacitor), $\eta_{out_2} = 0.91$ p.u. (battery), $C_{d_1} = 0.1$ p.u. (supercapacitor), $C_{d_2} = 1$ p.u. (battery), $\varepsilon_v = 0.01$ p.u., $k_g = 0.8$ p.u., $\alpha = 0.75$ p.u., $\beta = 0.25$ p.u., $n = 10$.

7. Acknowledgments

This work was supported by the Ministerio de Economia, Industria y Competitividad (Spanish government), under the grant agreement number ENE2017-86493-R.

References

[1] Renewable Capacity Statistics 2019, International Renewable Energy Agency (IRENA), March 2019 URL: `https://www.irena.org/publications/2019/Mar/Renewable-Capacity-Statistics-2019`. [Accessed on July 2021]
[2] Díaz-González F, Sumper A, Gomis-Bellmunt O. (2016) Energy storage in power systems. John Wiley and Sons, pp. 314
[3] Segundo Sevilla FR, Parra D, Wyrsch N, Patel MK, Kienzle F, Korba P. (2018) Techno-economic analysis of battery storage and curtailment in a distribution grid with high PV penetration. Journal of Energy Storage 17:73-83
[4] Lucas A, Chondrogiannis S. (2016) Smart grid energy storage controller for frequency regulation and peak shaving, using a vanadium redox flow battery. Electrical Power and Energy Systems 80:26-36
[5] Brijs T, Huppmann D, Siddiqui S, Belmans R. (2016) Auction-based allocation of shared electricity storage resources through physical storage rights. Journal of Energy Storage 7:82-92
[6] Troung CN, Schimpe M, Burger U, Hesse HC, Jossen A. (2018) Multi-use of stationary battery storage systems with blockchain based markets. Energy Procedia 155:3-16
[7] Grover-Silva E, Girard R, Kariniotakis G (2018) Optimal sizing and placement of distribution grid connected battery systems through an SOCP optimal power flow algorithm. Applied Energy 219:385-393
[8] Liu J, Chen X, Yang H, Li Y. (2020) Energy storage and management system design optimization for a photovoltaic integrated low-energy building. Energy 190:116424
[9] Georgiou GS, Christodoulides P, Kalogirou SA. (2020) Optimizing the energy storage schedule of a battery in a PV grid connected nZEB using linear programming. Energy 208:118177
[10] Nath S, Wu J (2020) Online battery scheduling for grid-connected photo-voltaic systems. Journal of Energy Storage 31:101713
[11] Cervone A, Carbone G, Santini E, Teodori E. (2016) Optimization of the battery size for PV systems under regulatory rules using a Markov-Chains approach. Renewable Energy 85:657-665
[12] Luo L, Abdulkareem SS, Rezvani A, Miveh MR, Samad S, Aljojo N, Pazhoohes M. (2020) Optimal scheduling of a renewable based microgrid considering photovoltaic system and battery energy storage under uncertainty. Journal of Energy Storage 28:101306
[13] Campana PE, Cioccolanti L, François B, Jurasz J, Zhang Y, Varini M, Stridh B, Yan J. (2021) Li-ion batteries for peak shaving, price arbitrage, and photovoltaic self-consumption in commercial buildings: A Monte Carlo Analysis. Energy Conversion and Management 234:113889
[14] Idlbi B, von Appen J, Kneiske T, Braun M (2016) Cost-Benefit analysis of battery storage system for voltage compliance in distribution grids with high distributed generation. Energy Procedia, 99:215-228
[15] Resch M, Bühler J, Klausen M, Sumper A. (2017) Impact of operation strategies of large scale battery systems on distribution grid planning in Germany. Renewable and Sustainable Energy Reviews 74:1042-1063

[16] Jing W, Hung Lai C, Wong WSH, Wong MLD (2018) A comprehensive study of battery-supercapacitor hybrid energy storage system for standalone PV power system in rural electrification. Applied Energy 224:340-356
[17] Ren G, Wang H, Chen C, Wang J (2021) An energy conservation and environmental improvement solution-ultra-capacitor / battery hybrid power source for vehicular applications. Sustainable Energy Technologies and Assessments 44:100998
[18] Sellali M, Betka A, Djerdir A (2020) Power management improvement of hybrid energy storage system based on H∞ control. Mathematics and Computers in Simulation 167:478-494
[19] Jing W, Hung-Lai C, Wong WSH, Wong MLD (2017) Dynamic power allocation of battery-supercapacitor hybrid energy storage for standalone PV microgrid applications. Sustainable Energy Technologies and Assessments 22:55–64
[20] Zhang Q, Wang L, Li G, Liu Y (2020) A real-time energy management control strategy for battery and supercapacitor hybrid energy storage systems of pure electric vehicles. Journal of Energy Storage 31:101721
[21] Hassani H, Zaouche F, Rekioua D, Belaid S, Rekioua T (2020) Feasibility of a standalone photovoltaic/battery system with hydrogen production. Journal of Energy Storage 31:101644
[22] Sinha S, Bajpai P (2020) Power management of hybrid energy storage system in a standalone DC microgrid. Journal of Energy Storage 30:101523
[23] Shayeghi H, Monfaredi F, Dejamkhooy A, Shafie-khah M, Catalao JPS (2021) Assessing hybrid supercapacitor-battery energy storage for active power management in a wind-diesel system. Electrical Power and Energy System 125:106391
[24] Prashant S, Singh Lather J (2021) Power management and control of a grid-independent DC microgrid with hybrid energy storage system. Sustainable Energy Technologies and Assessments 43:100924
[25] Bahloul M, Khadem SK (2020) An analytical approach for techno-economic evaluation of hybrid energy storage system for grid services. Journal of Energy Storage 31:101662
[26] Alvaro D, Arranz R, Aguado JA (2019) Sizing and operation of hybrid energy storage systems to perform ramp rate control in PV power plants. Electrical Power and Energy Systems 107:589-596
[27] Guentri H, Allaoui T, Mekki M, Denai M (2021) Power management and control of a photovoltaic system with hybrid battery-supercapacitor energy storage based on heuristics methods. Journal of Energy Storage 39:102578
[28] Deng Z, Hu X, Lin X, Che Y, Xu L, Guo W (2020) Data-driven state of charge estimation for lithium-ion battery packs based on Gaussian process regression. Energy 205:118000
[29] Deng Z, Hu X, Lin X, Che Y, Hu L (2020) General discharge voltage information enabled health evaluation for lithium-ion batteries. IEEE / ASME Transactions on Mechatronics 26:1295-1306
[30] European Commission (2016). Commission Regulation (EU) 2016/631 of 14 April 2016 establishing a network code on requirements for grid connection of generators. URL: `https://eur-lex.europa.eu/legal-content/EN/TXT/?uri=OJ\%3AJOL\_2016\_112\_R\_0001`. [Accessed on June 2020]
[31] Bullich-Massagué E, Aragüés-Peñalba, Sumper A, Boix-Aragones O. (2017) Active power control in a hybrid PV-storage power plant for frequency support. Solar Energy, Vol. 144, pp. 49-62
[32] Maxwell Technologies, ultracapacitor modules. URL: `https://www.maxwell.com/products/ultracapacitors/modules`. [Accessed on December 2021]
[33] Ultracell lead acid batteries catalogue. URL: `https://ultracell.co.uk/www.ultracell.co.uk/index.html`. [Accessed on December 2021]